Probing the Structure−Function Relationship of Polyene Macrolides: Engineered Biosynthesis of Soluble Nystatin Analogues

Sven E. F. Borgos,[†] Pascale Tsan,[‡] Håvard Sletta,[§] Trond E. Ellingsen,[§] Jean-Marc Lancelin,[‡] and Sergey B. Zotchev*[,†]

Department of Biotechnology, Norwegian University of Science and Technology, N-7491 Trondheim, Norway, RMN Biomoléculaire, Unité mixte de Recherche, Université Claude Bernard−Lyon 1, CNRS Sciences Analytiques, ESCPE, Lyon, F-69622 Villeurbanne, France, and Department of Biotechnology, SINTEF Materials and Chemistry, N-7034 Trondheim, Norway

Received September 11, 2005

Although polyene macrolides are efficient antifungal agents with fungicidal mode of action, their use in medical practice is problematic due to their low solubility and significant human toxicity. In an attempt to address the solubility problem, we have obtained two analogues of nystatin with hydroxy groups at positions C31 and C33 through manipulation of the nystatin polyketide synthase in the producing organism *Streptomyces noursei*. Structures of the analogues were confirmed by nuclear magnetic resonance (NMR), and their solubility was found to be more than 2000 times higher than that of nystatin. However, both analogues were shown to have lost antifungal activity, implying that the integrity of the hydrophobic polyene region of the nystatin molecule is crucial for the fungicidal action. NMR data and computer modeling performed for the new analogues suggested conformational changes together with a significantly increased structural disorder, which may account for both increased solubility and the loss of activity.

Introduction

A wide variety of biologically active compounds are synthesized as secondary metabolites by the polyketide synthase (PKS[a]) systems in *Streptomyces* bacteria.[1] These include substances with antibacterial,[2] antifungal,[3] antiparasitic,[4] immunosuppressive,[5] and antitumor[6] activities, to name but a few. The PKS-synthesized compounds, generally termed polyketides, are assembled by repeated condensation of small activated carboxylic acids such as malonyl- or methylmalonyl-CoA,[7] in a fashion similar to that of the fatty acid synthesis in both bacterial[8,9] and mammalian systems.[10] The PKS type I systems, which are responsible for biosynthesis of macrolide polyketides, are closer to the latter in the sense that all biosynthetic and reductive activities are ensured by distinct domains within the same multifunctional enzyme, whereas in bacterial fatty acid synthases (FAS) the system is dissociated and each step in the biosynthesis is performed by a discrete protein.[9] During the fatty acid synthesis by FAS, the same enzymatic sites are utilized repeatedly until the desired carbon chain length is reached, whereupon the chain is released from the enzyme complex by a thioesterase (TE). Type I PKS, like the erythromycin[2] and nystatin[3] PKS, are giant multifunctional proteins organized in modules where a separate set of enzymatic domains exists for each elongation step, i.e. each catalytic domain is used only once.[2,7] This makes the type I PKS architecture particularly amenable to genetic engineering aimed at production of novel polyketides.

* Corresponding author. Tel: +47 73 59 86 79. Fax: +47 73 59 12 83. E-mail: sergey.zotchev@nt.ntnu.no.

[†] Norwegian University of Science and Technology.

[‡] Université Claude Bernard Lyon 1.

[§] SINTEF Materials and Chemistry.

[a] Abbreviations: PKS, polyketide synthase; FAS, fatty acid synthase; TE, thioesterase; ACP, acyl carrier protein; KS, ketosynthase; AT, acyltransferase; KR, ketoreductase; DH, dehydratase; ER, enoyl reductase; HPLC, high-performance liquid chromatography; MS, mass spectroscopy; TOF, time-of-flight; Mw, molecular weight; DAD, diode-array detector; COSY, correlation spectroscopy; TOCSY, total correlated spectroscopy; ROESY, rotational nuclear Overhauser effect spectroscopy; ROE, rotational nuclear Overhauser effect; HSQC, heteronuclear single quantum correlation; HMBC, heteronuclear multiple bond correlation; rmsd, root-mean-square deviation.

The enzymatic reactions involved in both polyketide and fatty acid biosynthesis can be grouped into two main categories, the chain elongation steps and the reductive steps. The chain elongation is performed by three domains found in all PKS and FAS: the acyl carrier protein (ACP), the ketosynthase (KS), and the acyl transferase (AT). For each elongation step, the acyl unit is incorporated in the growing carbon chain with a β-keto functionality. This keto group can be reduced to a hydroxyl, a double bond, or a saturated single bond by the successive action of ketoreductase (KR), dehydratase (DH), and enoyl reductase (ER) domains, respectively.[7] The DH domains of PKS and FAS catalyze formation of an unsaturated double bond through elimination of water. This is usually a trans bond, but the alternative dehydratase FabA from the type II FAS of *Escherichia coli* is able to form a cis equivalent by isomerization.[11] As opposed to KR and ER domains, the DH does not require reductive energy, e.g. from NAD(P)H. The DH-catalyzed hydration−dehydration equilibrium has been shown to favor the substrate (hydrated) side by a factor of approximately 9:1 in assays of both *E. coli*[12] and mammalian cytosolic FAS,[13] making the overall reductive pathway dependent on the subsequent ER-catalyzed reaction to "pull" the substrate through. The His residue of the DH consensus sequence HxxxGxxxxP was suggested by Donadio and Katz[14] to be crucial for activity from their work on erythromycin PKS, and a corresponding His → Ala mutation in the DH domain of animal FAS completely eliminated dehydratase activity.[15] The latter observation pointed out this specific His residue as a target for mutagenesis that can be used to inactivate DH domains in type I PKS, subsequently resulting in the appearance of a hydroxy group at the β-carbon of the acyl unit incorporated into the polyketide chain by a previous module.

Polyene macrolides, the efficient antifungal agents, are synthesized by type I PKS in certain *Streptomyces* species.[16] The mode of action of these antibiotics, namely formation of the permeable channels in fungal membranes, is dependent on the interactions of antibiotic molecules with ergosterol.[17] Such interaction seems to occur through the polyene region containing a set of conjugated double bonds, which also provide for the

10.1021/jm050895w CCC: $33.50
Published on Web 03/23/2006

rigidity of the antibiotic molecules presumably important for channel stability.[18] At the same time, the high degree of hydrophobicity of the polyene region must contribute significantly to the low solubility of polyene macrolides, which creates problems with administration of these antibiotics. Recently, promising results have been obtained by conjugating amphotericin B to the highly water-soluble polysaccharides arabinogalactan[19] and *N*-methyl-*N*-D-fructose.[20] These derivatives were shown to have both antifungal activity and significantly increased solubility. However, these derivatives have not reached the market so far, probably due to high costs for their synthesis or unexpected side effects.

In the current study, we have attempted to produce soluble derivatives of the polyene macrolide nystatin by means of genetic engineering of the nystatin PKS in the bacterium *S. noursei* ATCC 11455. Two highly soluble nystatin analogues were produced, but they were shown to have lost all detectable antifungal activity. These data, along with the results from computer modeling performed for the new analogues, provide new insights into the structure−function relationship of the polyene macrolide antibiotics.

Results

Inactivation of the Active-Site His Residues in the DH3 and DH4 Domains of Nystatin PKS Results in Production of Novel Nystatin Analogues. The polyene region of nystatin A_1 contains sets of two and four conjugated double bonds spanning from C20 to C33 (Figure 1A). Although it was logical to assume that the whole polyene region is important for the interaction with ergosterol, there existed no experimental evidence for such a claim. Keeping in mind that decreasing the hydrophobicity of the polyene region might significantly increase solubility of the molecule, we decided to introduce hydroxyl groups at either position C31 or C33 by inactivating the DH domains in modules 3 and 4, respectively, on the nystatin PKS NysC. The putative active site His residues His935 (DH3) and His2681 (DH4) of NysC in the HxxxGxxxxP motifs (Figure 2) of the DH domains were changed to either tyrosine or alanine by site-specific mutagenesis, yielding the mutants $DH3_{H935Y}$, $DH3_{H935A}$, $DH4_{H2681Y}$, and $DH4_{H2681A}$. These mutations were introduced into the *nysC* gene in the nystatin nonproducing *nysA*-deficient strain NDA59[40] by means of suicide plasmids constructed for gene replacement (see Experimental Section) and subsequent selection for double homologous recombination. The DH mutations in *S. noursei* were verified by Southern blot analysis (data not shown). The selection of the DH3 mutants was based on the introduction of an additional *Bsr* GI restriction site into the DH3 coding region in the case of DH3(H64Y) mutant and the *Bsg* I restriction site in the case of the DH3-(H64A) mutant. Both DH4 mutants were selected on the basis of the introduction of the additional *Kpn* I restriction site into the DH4-coding region (see Experimental Section). Polyene macrolide production was then restored in the mutants by complementation with *nysA* gene expressed in trans from its own promoter using site-specific integration plasmid $pKS^{S}AT0$. We have previously shown that such complementation of the NDA59 strain restores nystatin production to the wild-type levels.[40]

Systems of conjugated double bonds generally exhibit very characteristic UV absorption spectra, with the absorption maxima wavelengths depending on the number of conjugations.[41] When the above mutant strains were grown in shake-flasks, the $DH3_{H935Y}$, $DH4_{H2681Y}$, and $DH4_{H2681A}$ mutants each showed production of one major tetraene. The M_w values of

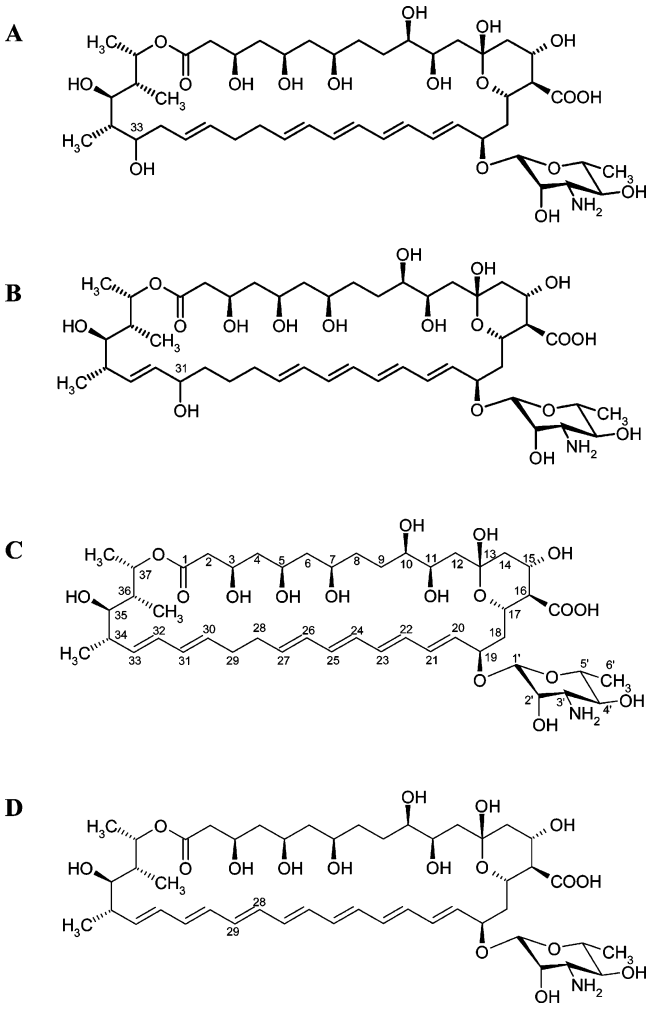

Figure 1. Chemical structures of the polyene macrolides nystatin and its hydroxy and S44HP analogues: (A) 33-hydroxynystatin, (B) 31-hydroxynystatin, (C) nystatin A_1. (D) S44HP.[42]

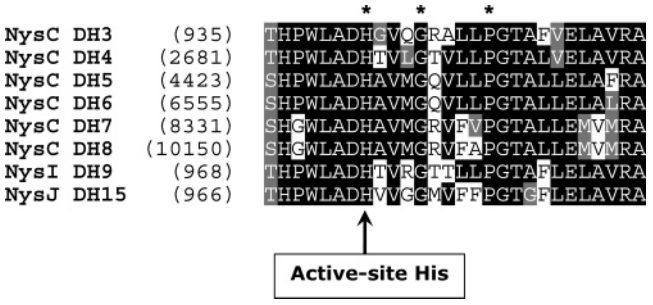

Figure 2. Alignment of regions encompassing active sites of the DH domains in nystatin PKS (3). Residues of active-site motif HxxxGxxxxP are marked with asterisks, and numbers in parentheses give positions of active-site His residues in the respective proteins.

these compounds were determined by HPLC/TOF-MS to be 942.5064 and 942.5068 Da for the DH3 mutant and DH4 mutants, respectively, both in excellent agreement with a stoichiometric formula of $C_{47}H_{76}NO_{18}$ for the $(M - H)^-$ ions, with a mass accuracy better than 0.32 ppm (data not shown). However, the polyene production levels were severely reduced compared to the wild-type, the $DH3_{H935Y}$ and $DH4_{H2681A}$ mutants yields being approximately 1.5% and 3.0% of the wild-type nystatin level, respectively. The $DH4_{H2681Y}$ mutant produced somewhat less polyene than the $DH4_{H2681A}$, even though the production and cell extract profile was qualitatively similar as judged from HPLC/MS. Thus, the $DH4_{H2681Y}$ mutant was not

Table 1. Bacterial Strains, Plasmids, and Phages Used in This Study

strain or plasmid	description	source or reference
	E. coli	
DH5α	general cloning host	BRL
ET12567 (pUZ8002)	strain for intergeneric conjugation	22
	S. noursei	
ATCC 11455	wild-type strain, nystatin producer	ATCC
NDA59	mutant strain with *nysA* in-frame deletion, nystatin nonproducer	40
	Plasmids and Phages	
N14	recombinant λ phage, nystatin cluster encompassing upstream part of *nysC*	3
pLITMUS28	general cloning vector	New England Biolabs
pGEM3zf(−)	general cloning vector	Promega
pGEM7zf(−)	general cloning vector	Promega
pSOK201	*E. coli*−*S. noursei* conjugative vector	46
pL14X	14.3 kb *Xba* I fragment from phage N14 cloned in pGEM3zf(−)	3
pDH3	3.9 kb *Sph* I fragment from pL14X cloned in pGEM7zf(−)	this study
p699DH3	699 bp *Bsi* WI−*Nco* I fragment from pDH3 cloned in pLITMUS28	this study
pSOKDH3/H64Y	construct for gene replacement in *nysC* with His935Tyr mutation in the DH3 coding region	this study
pSOKDH3/H64A	construct for gene replacement in *nysC* with His935Ala mutation in the DH3 coding region	this study
pDH4	3.6 kb *Sph* I fragment from pL14X cloned in pGEM7zf(−)	this study
p766DH4	766 bp *Asc* I−*Nco* I fragment from pDH4 cloned in *Bss* HII and *Nco* I sites of pLITMUS28	this study
pSOKDH4/H65Y	construct for gene replacement in *nysC* with His2681Tyr mutation in DH4 coding region	this study
pSOKDH4/H65A	construct for gene replacement in *nysC* with His2681Ala mutation in DH4 coding region	this study
pKSSAT0	nysA under own promoter in integration plasmid for complementation of *S. noursei* NDA59	40

included in further analysis. Notably, the $DH3_{H935A}$ mutant produced only trace amounts of polyene macrolides, suggesting that the two DH domains responded differently to the chosen active-site residue alterations. No nystatin A_1 production could be detected in any of the mutants, demonstrating the complete abrogation of the targeted dehydratase activity.

942.5 Da Nystatin Analogues Contain an Additional Hydroxyl Group at Expected Positions. The two tetraene macrolides with $M_w = 942.5$ Da, one from each of the $DH3_{H935Y}$ and $DH4_{H2681A}$ mutants, were purified on a preparative scale and subjected to NMR structure elucidation (see Experimental Section). Presumably, these mutants should produce the nystatin analogues 33-hydroxynystatin and 31-hydroxynystatin, respectively, and the NMR results obtained for the purified compounds were fully consistent with the expected structures. The observed ^1H and ^{13}C NMR data are given in Table 2, and ^1H chemical shift changes relative to nystatin A_1[18] are shown in Figure 3. For the compound isolated from the $DH3_{H935Y}$ mutant, a large upfield shift was found at C32 and C33, both in the ^1H and ^{13}C spectra (Figure 5 and Figure S1 in Supporting Information). As shown in Figure 3, significant shifts were also detected, especially in the ^1H spectra, for the whole C31 to C35 region and, notably, for C37. For the rest of the molecule, there were only minor changes compared to nystatin signals as reported by Volpon and Lancelin.[18] The observed signals were very well

Table 2. ^1H and ^{13}C Chemical Shifts for 33-Hydroxynystatin and 31-Hydroxynystatin in Methanol-d_4 at 25 °C[a]

	33-hydroxynystatin		31-hydroxynystatin	
position	δ ^1H (ppm)	δ ^{13}C (ppm)	δ ^1H (ppm)	δ ^{13}C (ppm)
2	2.39	43.8	2.42	42.6
3	4.13	67.6	4.19	67.0
4	1.65	44.0	1.60	44.0
5	3.99	69.8	3.99	69.4
6	1.56	43.7	1.45	43.7
7	3.80	70.3	3.80	71.1
8,9	1.61	28.8	1.45	29.0
10	3.40	69.3	3.16	69.3
11	4.06	71.0	4.00	71.9
12			1.65, 1.90	43.9
13				
14	1.34, 2.05	43.7	1.32, 2.06	44.0
15	4.25	66.7	4.26	69.7
16	2.09	59.4	2.07	59.9
17	4.06	67.2	4.27	69.7
18	1.83, 1.93	39.0	1.78, 2.07	38.9
19	4.44	78.2	4.44	78.1
20	5.69	134.8	5.89	134.3
21	6.33	132.3	6.22	131−133
22−25	6.23	132.3	6.30	131−133
26	6.10	131.2	6.13	131.2
27	5.73	133.4	5.70	134.3
28	2.19	32.9	2.12	32.7
29	2.14	32.7	1.44	
30	5.52	132.3	1.41	
31	5.52	127.3	3.96	72.7
32	2.20, 2.33	38.4	5.43	132.9
33	3.58	74.2	5.62	135.1
34	1.63	38.5	2.37	40.7
34-CH_3	0.90	8.9	1.06	16.0
35	3.85	73.9	3.28	77.3
36	1.71	42.3	1.99	40.6
36-CH_3	0.74	10.2	0.97	11.3
37	4.00	69.8	5.23	71.9
37-CH_3	1.12	17.7	1.20	16.5
1	4.61	98.8	4.59	98.3
2	3.99	68.3	4.00	68.2
3	3.17	56.1	3.16	56.1
4	3.40	69.3	3.39	69.3
5	3.29	73.5	3.30	73.6
6	1.28	16.9	1.28	16.8

[a] Accuracy of the chemical shifts measured are ±0.02 ppm for ^1H and ±0.2 ppm for ^{13}C.

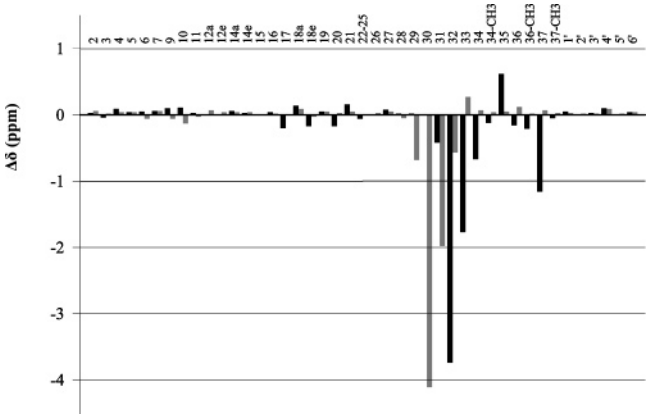

Figure 3. Change in the ^1H chemical shift (Δδ) for 33-hydroxynystatin (black) and 31-hydroxynystatin (gray) relative to nystatin A_1.

in accordance with the structure of the predicted 33-hydroxynystatin (Figure 1B).

For the $M_w = 942.5$ Da compound from the $DH4_{H2681A}$ mutant, large upfield shifts relative to nystatin A_1 were found for C30 and C31 (Figure 3). Somewhat smaller, but yet significant, shifts were observed for C29, C32 and C33, whereas the rest of the spectrum showed only minor differences from

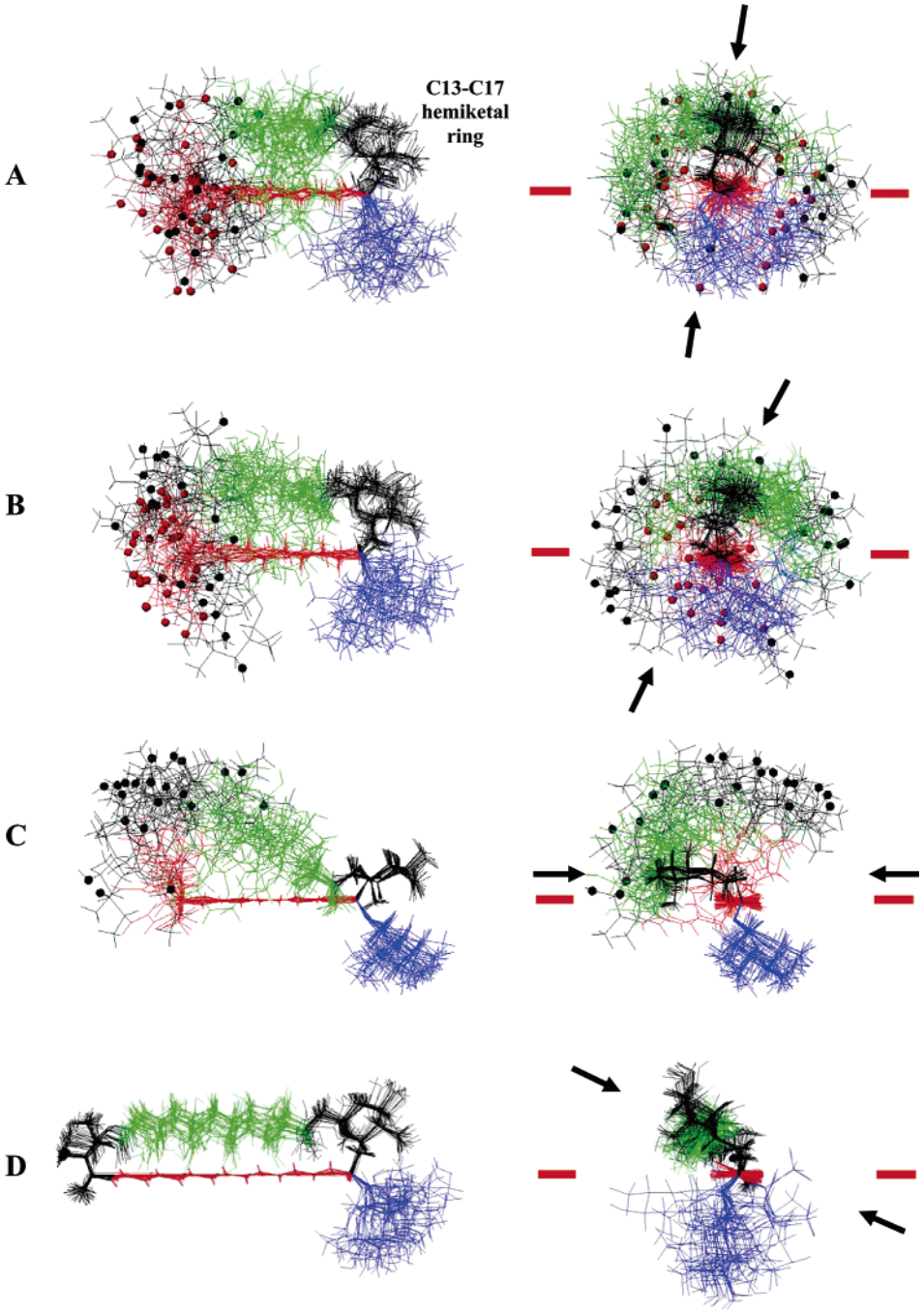

Figure 4. NMR-restrained model structures of nystatin A_1 and its hydroxy and S44HP analogues: (A) 33-hydroxynystatin, (B) 31-hydroxynystatin, (C) nystatin A_1,[18] and (D) S44HP. Twenty-four structures of each molecule are superposed for a minimal rmsd considering the backbone heavy atoms of the C11−C27 segment for 33-hydroxynystatin, 33-hydroxynystatin, and nystatin A_1 and extended to C11−C33 for S44HP. Left: View with the tetraene plane lying horizontally and the mycosamine moiety pointing down. Right: Side view with the mycosamine moiety in front. Blue: Mycosamine moiety. Red: Polyene region (C20−C33). Green: Polyol region (C1−C11). Black ball: O atom of OH group on C35. Red ball: O atom of new OH group on the nystatin analogues (on C33 or C31, respectively). The black arrows and the red lines indicate the equatorial plane of the hemiketal C13−C17 ring and the C20−C27 tetraene plane, respectively.

that of nystatin A_1. The spin systems observed are well in accordance with the expected structure of 31-hydroxynystatin (Figure 1C). Interestingly, the chemical shift for C37 was very similar to that of nystatin A_1, in stark contrast to what was observed in the spectra of putative 33-hydroxynystatin as mentioned above.

Taken together, the DAD, TOF-MS, and NMR data unambiguously identify the analyzed compounds as 33-hydroxynystatin from the $DH3_{H935Y}$ mutant and 31-hydroxynystatin from the $DH4_{H2681A}$ mutant.

Addition of Hydroxyl Group to C31 or C33 of Nystatin Significantly Increases Water Solubility. The polyene region of nystatin is very unpolar, supposedly promoting hydrophobic interactions between this region and sterols within the cell membrane and orienting the polyol part of the molecule toward the internal aqueous channel.[17] However, this low polarity also leads to significant difficulties in administration during human therapy.

To investigate the influence of introduced hydroxyl groups on the properties of newly obtained nystatin analogues, we tested

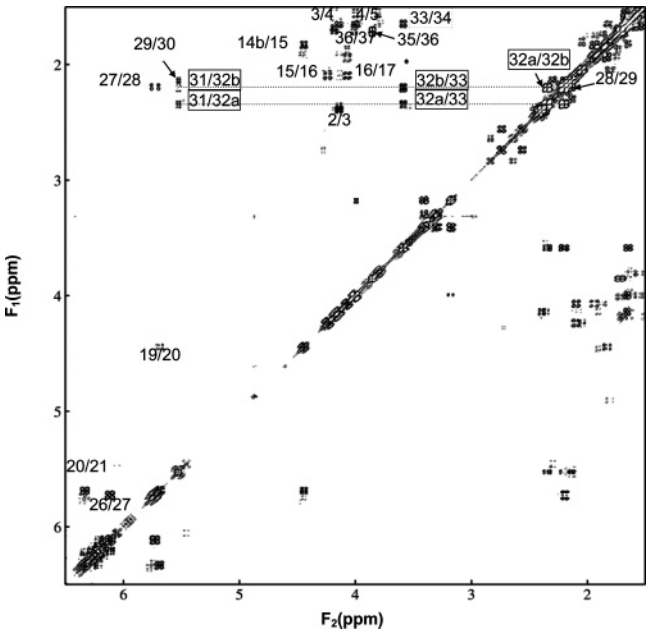

Figure 5. COSY region of 33-hydroxynystatin showing connectivities (with framed numbers) from the protons at the modified C32−C33 positions. For CH_2 groups, nonequivalent geminal protons are referred to as "a" and "b". The chemical shifts corresponding to the C32 geminal protons are marked by dotted lines.

the solubility of the purified compounds, as well as the nystatin A_1 reference, in an aqueous buffer solution of 10 mmol Tris-HCl, pH 7.0 by spectrophotometric methods (see Experimental Section). For nystatin under our conditions, we found the solubility to be 0.11 mg/mL, whereas the 31- and 33-hydroxy analogues gave values of 377 and 291 mg/mL, respectively. This surprisingly high solubility of the nystatin analogues was subsequently confirmed by gravimetric methods (see Experimental Section). HPLC/MS analysis showed that 33-hydroxynystatin appeared to be somewhat unstable in aqueous solution, even though the corresponding molecular ion was still the dominant one in the mass spectra after approximately 4 h of incubation in the buffer solution at room temperature. For 31-hydroxynystatin, no such instability was observed. The high aqueous solubility of the nystatin analogues was in accordance with our observations that both compounds are significantly less retained on a reverse-phase HPLC column than nystatin A_1 under similar conditions (data not shown). We have also observed in fermentations that, for the DH3 and DH4 mutants, a considerable fraction of the total polyene macrolides was found dissolved in the fermentation medium, while for the wild-type, almost all nystatin was associated with the cell pellet and the dissolved concentration was negligible (data not shown).

31- and 33-Hydroxynystatins Have No Detectable Antifungal Activity against *Candida albicans*. Keeping in mind that the polyene region of nystatin and the other antifungal polyene macrolides is thought to interact specifically with membrane sterols, one would expect the addition of a hydroxyl group on C31 or C33 to influence the biological activity of the molecules. To assess the antifungal potency of the new analogues, we performed bioactivity assays with *C. albicans* ATCC 10231 as described previously.[42] The MIC_{50} for nystatin was found to be 0.48 μg/mL under the conditions tested, whereas for the 31- and 33-hydroxy derivatives, no inhibition of fungal growth could be detected up to 200 μg/mL, the highest analogue concentration tested. These data clearly show that introduction of either C33 or C31 hydroxyls with subsequent elimination of C30−C31 or C32−C33 double bonds, respectively, is detrimental for the antifungal activity of nystatin.

NMR-Restrained Modeling of the New Nystatin Analogue Molecules Suggests Higher Level of Structural Disorder. Volpon and Lancelin[18] have previously described simple structure calculations and modeling of the structure for nystatin A_1 and four other glycosylated polyene macrolides based on NMR data. We have used a similar approach and protocols for analysis of the NMR data obtained for the 31- and 33-hydroxynystatin analogues. Fifty structures were generated for each analogue, using 78 distance and 2 dihedral angle restraints for the 33-hydroxynystatin, and 38 distance and 4 dihedral angle restraints for the 31-hydroxynystatin (see Supporting Information, Table S1). Twenty-four structures of low energy were retained for each analogue. The average total potential energy was 9.82 ± 0.46 kcal.mol^{-1} for 33-hydroxynystatin and 8.42 ± 0.06 kcal mol^{-1} for 31-hydroxynystatin, which was similar to the value of 7.85 ± 0.42 found for nystatin A_1.[18] No distance or dihedral angle restraint violations were found. The 24 structures were superposed (Figure 4) for each derivative in MOLMOL[39] considering the backbone heavy atoms of the C11−C27 region only, as done for nystatin A_1. The corresponding root-mean-square deviation (rmsd), which was 0.17 ± 0.05 Å in nystatin A_1, was found to be 0.75 ± 0.32 Å in 33-hydroxynystatin and 0.88 ± 0.40Å in 31-hydroxynystatin. These significantly higher, compared to nystatin A_1, rmsd values presumably reflect a higher level of structural disorder for the two nystatin analogues.

NMR-Restrained Modeling of the Heptaene S44HP Nystatin Analogue with High Antifungal Activity Suggests a High Global Structural Order. S44HP is an analogue of nystatin A_1 produced by the ERD44 mutant,[42] where an enoyl reductase domain in the module 5 of the nystatin PKS is inactivated. S44HP contains a C28−C29 double bond, instead of a C28−C29 single bond in nystatin A1, thus representing a heptaene analogue of the latter macrolide (Figure 1D). It has been shown that S44HP displays approximately 6 times higher antifungal activity compared to nystatin against the same strain of *Candida* under the same assay conditions which were used in this work.[42] Similar structure calculations for S44HP, using 34 distance restraints and 5 angle restraints, led to 24 structures with an average total energy of 6.97 ± 0.22 kcal mol^{-1}. The region considered for the superposition could be extended to the C11−C33 segment structures and the corresponding rmsd was found to be 0.30 ± 0.15 Å. As shown on Figure 4D, the molecule is globally much better defined, the disordered regions being limited to the polyol region and the mycosamine.

Discussion

In an attempt to produce analogues of the polyene macrolide antibiotic nystatin with increased solubility, two recombinant strains of *S. noursei* with inactivated DH domains in modules 3 and 4 of the nystatin polyketide synthase were constructed. The DH mutants were shown to produce nystatin analogues with an additional hydroxyl group on either C33 or C31 at significantly reduced levels compared to production of nystatin by the wild-type strain. Since the growth of the mutants was not impaired to any measurable degree, it seems unlikely that the new derivatives are toxic to the producing organisms. The reason for the yield reduction must then be sought elsewhere, and it seems reasonable to assume that it may be due to suboptimal substrate recognition by the subsequent downstream ketosynthase domains KS4 and KS5. Witkowski et al.[13] have shown that for mammalian cytosolic FAS, the DH domain catalyzes

the reverse (hydration) reaction much more efficiently than the forward (dehydration) reaction. The same could also be true for PKS systems, based on functional similarity and the general rule that enzymes do not alter the equilibrium of catalyzed reactions, only accelerating the attainment of such equilibrium. Taking into account that neither module 3 nor module 4 of the nystatin PKS contains the ER domain, we presume that even in the wild-type PKS, the KS4 and KS5 should be faced with a majority of substrates with β-hydroxyl functionality. However, neither C31- nor C33-hydroxynystatin analogues could be identified in detectable amounts in the wild-type extracts (unpublished data), suggesting that the KS4 and KS5 prefer the substrates with β-methylene functionality.

The purified 33- and 31-hydroxynystatin derivatives both displayed a strong (more than 2000-fold) increase in aqueous buffer solubility. Increasing polyene solubility for easier clinical administration was part of the rationale for constructing the above mutants in the first place and was expected, considering the increased polarity of a hydroxyl group compared to a double bond. Still, such a drastic increase in solubility was surprising, and most probably cannot be attributed solely to the change of polarity due to the introduction of one extra hydroxyl group. Polyene macrolides are known to form aggregates in aqueous solutions,[43,44] and it is logical to assume that such aggregates might form through intermolecular hydrophobic interactions involving the polyene region.[45] We therefore suggest that disruption of the polyene region in the new nystatin analogues greatly reduces their ability to form aggregates, thereby significantly enhancing solubility.

The loss of antifungal activity by the 31- and 33-hydroxynystatins shown in the *C. albicans* assays was not as easily predictable. In part, the loss of activity could be due to the disturbance of the hydrophobic interactions that are presumed to direct the polyene region of the antibiotic toward membrane sterols and facilitate the formation and stabilization of transmembrane channels.[45] Possibly, there could also be an element of sterical hindrance of the polyene macrolide−sterol interaction, due to the introduced hydroxyl group being significantly larger than the native sole hydrogen atom. Disruption of aggregate formation could also account for the loss of activity, since it is conceivable that such aggregates are required for creating a critical concentration of antibiotic on the surface of the membrane, thereby ensuring membrane penetration and formation of a channel.[45]

The new chemical groups introduced in the 31- and 33-hydroxynystatin analogues afford two additional free rotations around the consequently saturated C−C bonds in the C30−C33 region. These new degrees of freedom in the nystatin structure could induce different conformations. Like in nystatin A_1,[18] it is probable that the populations of the different possible conformers will be influenced by solvatation either in aqueous or hydrophobic (lipid) environment. In methanol, we observed significant NMR differences, manifested as qualitative and relative different ROE intensities or different *J*-coupling patterns in the C17−C19 region. This observation supported differences in the conformational behavior of the 31- and 33-hydroxynystatin derivatives. Using the same simple NMR-restrained modeling protocols as used for nystatin A_1, we found consequently a different conformation of the C13−C17 hemiketal ring relative to the C20−C27 tetraene plane. The equatorial plane of the C13−C17 hemiketal ring appears tilted relative to the tetraene C20−C27 plane in the hydroxy analogues, while being parallel in nystatin A_1 as shown in Figure 4. The simplistic calculated models also show that the polar groups of the polyene macrolides are clustered on the same side of the molecule in nystatin A_1, in accordance with its amphiphilic nature. This feature is no longer apparent in the models of the 31-hydroxy and 33-hydroxynystatins (Figure 4).

Volpon and Lancelin[18] have previously reasoned that the saturated C28−C29 single bond in nystatin is a possible source for the increase in conformational variation seen when nystatin models are compared with those of polyene macrolides with a fully conjugated set of double bonds, like amphotericin B, pimaricin, or candicidin. By analogy, we would expect the further removal of double bonds, as described for the new nystatin analogues, to allow for even more flexibility and structural disorder. Moreover, the hydrophobic/hydrophilic balance is significantly perturbed in these derivatives, since a double bond in the hydrophobic polyene region in these analogues is replaced by a hydrophilic group. This leads to a very limited hydrophobic core compared to the mainly hydrophilic parts of macrolactone ring surrounding it and thus to a significant decrease in the amphiphilic character of this macrocycle (Figure 4A,B). The latter could account for the astonishing increase in water solubility, together with the loss of activity that is indeed related to the ability of the molecules to interact with the highly hydrophobic sterols and to form channels.

This interpretation can be supported by the results on the fully conjugated heptaene or octaene derivatives of nystatin isolated and characterized previously.[42] The latter compounds possess on the contrary a longer polyene region, representing nearly half of the molecule, and have been shown to be more active than the native nystatin A_1. Structure modeling for the heptaene S44HP analogue gave relatively well ordered models with a conformation nearly identical to the heptaene candidin[18] (Figure 4D). Candinin actually differs from S44HP, in terms of the macrolactone ring, only by a keto group instead of a hydroxy group at C7 in the polyol region. The results suggest that the presence of this longer and more rigid polyene region allows a very defined amphiphilic structure with one entirely hydrophobic side constituted by the heptaene and an opposite side mainly hydrophilic (Figure 4D). The ratio between the length of the hydrophobic region and the hydrophilic region is indeed close to 1, whereas the hydrophilic character was largely dominant in the 31- and 33-hydronystatin derivatives and tended to conceal the hydrophobic character of the macrocycles. Taken together, our experimental and modeling studies suggest that the hydrophobic/hydrophilic ratio is a crucial factor for the antifungal activity of polyene macrolides, since the reduction of the length of the polyene hydrophobic region seems to be correlated to a decrease of activity, probably related to a decrease of its propensity to form channels. Last, this hypothesis can be corroborated by the observation that other polyene macrolide antibiotics with antifungal activity,[18] including smaller ones such as the tetraene pimaricin, all have in common these amphiphilic properties with similar ratios between the polyene and the hydrophilic region.

Significance. Polyene macrolides are efficient antifungal agents the use of which is limited due to significant toxicity and low solubility. Having access to the polyene macrolide biosynthetic genes opens new possibilities for production of polyene macrolides with potentially improved pharmacological properties. Two novel analogues of the polyene macrolide antifungal antibiotic nystatin with altered polyene region have been produced upon manipulation of the nystatin polyketide synthase in the bacterium *S. noursei*. Both analogues, the identities of which were confirmed by NMR as 33- and 31-hydroxynystatins, exhibited over 2000-fold increase in aqueous

solubility compared to nystatin. However, the analogues have lost their antifungal activity against *C. albicans*, pointing out the significance of the intact polyene region for this activity. Modeling of the solution structures for the two new nystatin analogues based on the NMR data suggested conformational changes that explain the properties of these compounds. The data obtained provide new insights into the structure−function relationship of polyene macrolides and may assist in engineered biosynthesis of new antifungal drugs.

Experimental Section

Bacterial Strains, Media, and Growth Conditions. Plasmids, strains, and phages used are described in Table 1. All handling and propagation of *Escherichia coli* strains were done according to standard procedures.[21] Conjugal transfer of plasmids from *E. coli* ET12567(pUZ8002) to *S. noursei* and gene replacement procedures were performed as described previously.[22,23] When required, antibiotic selection was done with the following concentrations: ampicillin, 100 μg/mL; apramycin, 50 μg/mL; chloramphenicol, 20 μg/mL; kanamycin, 50 μg/mL, nalidixic acid, 30 μg/mL. *S. noursei* strains were grown on solid ISP2 agar medium (Difco) and in liquid TSB (tryptone soy broth) medium (Oxoid) for genomic DNA isolation. High-pressure liquid chromatography with mass spectroscopy (HPLC/MS) analysis of polyene production by *S. noursei* strains was performed on cultures grown in 500-mL shake flasks of liquid SAO-23 medium.[23] Growth in 3-L fermentors was done essentially as described previously.[23]

DNA Manipulation, Sequencing, and Sequence Analysis. The DNA sequence for the nystatin gene cluster has been reported previously.[3] General DNA manipulation was done as described elsewhere.[21] Purification of DNA fragments from agarose gels and isolation of genomic *S. noursei* DNA was done with the QIAEX II Kit and DNEasy Tissue Kit, respectively (both QIAGEN). Probes for Southern blot analysis were made with the PCR DIG Probe Synthesis Kit (Roche Molecular Biochemicals) according to the manufacturer's instructions. Site-specific mutagenesis was performed using the QuikChange II Site-Directed Mutagensis Kit (Stratagene) on a Mastercycler Gradient (Eppendorf) PCR machine, with oligonucleotide primers from Operon Biotechnologies. All other oligonucleotides were purchased from MWG Biotech. DNA sequencing was done with the ABI Prism Big Dye Terminator Cycle sequencing kit and a Genetic Analyzer 3100 (Applied Biosystems).

Construction of Plasmids for Introduction of Point Mutations. DH3 Mutants. A 14.3 kb *Xba* I fragment from phage N14 encompassing the upstream part of *nysC* was cloned into the *Xba* I site of pGEM3zf(−), giving plasmid pL14X. This plasmid contains the gene regions corresponding to the entire modules 3 and 4 of nystatin PKS. From pL14X, a 3.9 kb *Sph* I fragment was cloned in the corresponding site of pGEM7zf(−) to give plasmid pDH3. From this plasmid, a 699 bp *Nco* I−*Bsi* WI fragment was subcloned into same sites of pLitmus28 vector to yield mutagenesis template p699DH3. After site-specific mutagenesis with primer pairs DH3-(H64Y)−*Bsr* GI-f/-r and DH3(H64A)-f/-r and subsequent confirmation by sequencing, the mutagenized fragments were cloned back into pDH3, and the 3.9 kb insert from pDH3 was cloned into *Sph* I in pGEM3zf(−) to introduce suitable flanking restriction sites. These mutagenized inserts were finally ligated at *Bam* HI−*Hin* dIII with a 3.0 kb fragment of pSOK201 to yield replacement vectors pSOKDH3/H64Y and pSOKDH3/H64A, respectively.

DH4 Mutants. From the above pL14X plasmid, a 3.6 kb *Sph* I fragment was cloned in the *Sph* I site of pGEM7zf(−) to yield plasmid pDH4. A 766 bp *Asc* I−*Nco* I fragment was further subcloned in the *Bss* HII and *Nco* I sites of pLitmus28. The resulting plasmid p766DH4 was mutagenesis template for primer pairs DH4-(H65Y)-f/-r and DH4(H65A)-f/-r. After mutagenesis and subsequent confirmation by sequencing, the respective 766 bp fragments were cloned back into pDH4. The mutagenized 3.6 kb inserts of pDH4 were cloned into *Sph*I of pGEM3zf(−), re-excised by *Eco* RI−*Hin* dIII, and ligated via the corresponding sites of a 3.0 kb pSOK201 fragment to yield replacement vectors pSOKDH4/H65Y and pSOKDH4/H65A, respectively.

Primers for Site-Specific Mutagenesis. DH3 Mutants. To change the residue His935 of NysC to Tyr935 and Ala935, the following primer pairs were used, respectively: DH3(H64Y)-*Bsr*GI-f, 5′-GGCTCGCCGAC**T**ACGG**T**GT**ACA**GGGCCGGGC-3′ (sense); DH3(H64Y)-*Bsr*GI-r, 5′-GCCCGGCCCTG**T**AC**A**CCGT**A**GTCGGCGAGCC-3′ (antisense); and DH3(H64A)-f, 5′-GCTCGCCGAC**GC**CGGGGT**G**CAGGGCCGGG-3′ (sense); DH3(H64A)-r, 5′-CCCGGCCCTG**C**ACCCCG**GC**GTCGGCGAGC-3′ (antisense). The mutated nucleotides are shown in boldface, and the introduced restriction sites (*Bsr* GI and *Bsg* I, respectively) are underlined.

DH4 Mutants. To change the residue His2681 of NysC to Tyr2681 and Ala2681, the following primer pairs were used, respectively: DH4(H65Y)-f, 5′-CTGGCCGAC**T**ACACCGTCCTGGG**T**ACCGTCCTGC-3′ (sense); DH4(H65Y)-r, 5′-GCAGGACGGTA**C**CCAGGACGGTGT**A**GTCGGCCAG-3′ (antisense); and DH4(H65A)-f, 5′-CTGGCCGAC**GC**CACCGTCCTGGG**T**ACCGTCCTG-3′ (sense); DH4(H65A)-r, 5′-CAGG ACGGTA**C**CCAGGACGGTG**GC**GTCGGCCAG-3′ (antisense). The mutated nucleotides are shown in boldface, and the introduced restriction sites (*Kpn* I) are underlined.

HPLC/MS Analysis of Polyene Macrolides. Polyenes were extracted from shake-flask cell pellets with MeOH and analyzed by HPLC/MS on an Agilent 1100 HPLC system with a diode-array detector (DAD) and an Agilent MSD time-of-flight (TOF) mass spectrometer. Electrospray ionization was utilized both in the positive and negative mode. The HPLC column was a Waters NovaPak C_{18} with dimensions 2.1 × 150 mm run at a flowrate of 300 μL/min, and the mobile phase was a linear gradient from 40% to 65% MeOH in 10 mmol ammonium acetate, pH 4.0.

Preparative Purification of 31- and 33-Hydroxynystatin Analogues. Cultures of the mutant strains after fermentation were subjected to centrifugation. The cell pellets were extracted directly with methanol (MeOH), while the supernatants were freeze-dried under vacuum before MeOH extraction. The extracts were pooled and subjected to gel filtration chromatography (GFC) on a 22 × 850 mm column of ToyoPearl HW40-S material (TosoHaas) with MeOH as a mobile phase at a flow of 1.6 mL/min. The chromatographic system Pharmacia FPLC including a fraction collector and a UV detector at 254 nm was used. The relevant fractions were dried under vacuum, resuspended in a small amount of MeOH, and subjected to preparative reverse-phase HPLC on a Waters NovaPak C_{18} 30 × 300 mm column. Preparative HPLC was done two times for each compound, with different mobile phases to give orthogonal selectivity on the column. The first mobile phase was a linear gradient of 47.5% to 67.5% MeOH in 10 mmol ammonium acetate, pH 4.0, and the second was a linear gradient of 21% to 29% acetonitrile in the same buffer. The flow rate was 60 mL/min in both cases, and the column temperature was kept at 35 °C. This chromatography was done on an Agilent 1100 HPLC system with a flow split and molecular mass monitoring on an attached Agilent MSD Trap SL mass spectrometer. Fraction collection was done manually. The relevant fractions obtained after HPLC purification were extracted with solid-phase extraction cartridges (Waters Oasis HLB, 6 g) according to the manufacturer's instructions and eluted with MeOH. The final eluates were then dried under vacuum. The purity was >98% for both compounds purified, as assessed by analytical HPLC/MS.

NMR Experiments. 33-Hydroxynystatin (6 mmol) and 31-hydroxynystatin (14 mmol) NMR samples were obtained by dissolving under dry argon these derivatives in methanol-d_4. All NMR spectra were recorded at 25 °C on a Bruker Avance DRX 500 (^{1}H at 500.125 MHz, ^{13}C at 125.76 MHz) spectrometer using a 5-mm (^{1}H, ^{13}C, ^{15}N) triple-resonance probe head, equipped with a supplementary self-shielded *z*-gradient coil. As for nystatin A_1,[18] homonuclear two-dimensional experiments double-quantum filtered correlation spectroscopy (DQF-COSY),[24] total correlation spectroscopy (TOCSY), Hartmann−Hann spectroscopy,[25,26] and rotating Overhauser effect spectroscopy (ROESY)[27,28] were recorded with a 1.5-s recovery delay in the phase-sensitive mode using the States-

TPPI (time proportional phase incrementation) method[29] with 512 (t_1) × 1024 (t_2) complex data points. They were recorded with 32 scans per increment and spectral widths of 4500 Hz in both dimensions. Mixing time of 80 ms was used for the TOCSY experiments and 250 ms for the ROESY. Spectra were processed using GIFA V.4 software.[30] Data were apodized with shifted sine-bell and Gaussian window functions in both dimensions, after zero-filling in the t_1 dimension, to obtain a final matrix of 1024 (F_1) × 1024 (F_2) real data points. Chemical shifts were referenced relative to the solvent chemical shifts (^{1}H = 3.31 ppm). ^{1}H−^{13}C heteronuclear two-dimensional spectra included phase-sensitive ^{13}C-HSQC,[31] recorded using the echo-antiecho method,[32] and an additional ^{13}C-HMBC[33] to confirm the structure. The coherence pathway selection was achieved by applying pulsed-field gradients as coherence-filters.[34,35] Spectra were collected with 128 (t_1, ^{13}C) and 1024 (t_2, ^{1}H) complex points and 360 scans per t_1 increment, typically. Spectral widths were 17605 Hz in F_1 and 4496 Hz in F_2 with carrier frequencies at 70 and 3.5 ppm, respectively. Data were processed using PIPP software.[36] They were apodized with shifted square sine-bell window and Gaussian functions, respectively, in F_1 and F_2 dimensions, after linear prediction and zero-filling in the t_1 dimension to obtain a final matrix of 512 (F_1) × 1024 (F_2) real data points.

NMR Restraints and Structure Calculations. Interproton distance restraints were derived from two-dimensional homonuclear ROESY experiments and classified into three categories. Upper bounds were fixed at 2.7, 3.3, 5.0, and 6.0 Å for strong, medium, weak, and very weak correlations, respectively. The lower bound for all restraints was fixed at 1.8 Å, which corresponds to the sum of the hydrogen van der Waals' radii. The intensities of the ROE correlations of the H_i and H_{i+2} within the polyene part or the resolved methylene pairs at C14 were considered as reference intensities for strong correlations (see ref 18 and references therein). Pseudoatom corrections[37] of the upper bounds were applied for distance restraints involving unresolved methylene and methyl protons (+1 Å). For nonstereospecifically assigned but spectroscopically resolved diastereotopic protons, the interproton distances were treated as single $\langle r^{-6}\rangle^{-1/6}$ average distances. When possible, the H−C−C−H dihedral angle was restrained to dihedral domains according to the $^3J_{HC,CH}$ coupling constants measured using optimized Karplus dihedral relations.[18] Models were calculated using the X-PLOR software version 3.851.[38] Initial atomic coordinates and structure files for each derivative were obtained starting from those of nystatin A_1,[18] and similar calculation protocols were applied. The new stereogenic center created on nystatin hydroxy analogues were arbitrary fixed to *S*. The results were visualized using the program MOLMOL, version 2.4.[39]

Solubility Testing. Stock solutions of nystatin A_1 (Alpharma, UPS grade) standard (1.2 mg/mL) and the purified 31- and 33-hydroxy analogues (12 mg/mL) were prepared in methanol. A 100 μL portion of each stock was freeze-dried under vacuum for 24 h. To the dry polyenes was added either 50 μL (nystatin A_1) or 2 μL (31- and 33-hydroxynystatin) of aqueous 10 mmol Tris-HCl buffer, pH 7.0, and the solution was saturated by extensive (>15 min) vortexing. Polyene concentrations in solution were then determined by measuring UV absorbance spectra on a Perkin-Elmer Lambda 35 UV/vis spectrophotometer after appropriate dilution. Specifically, the characteristic tetraene UV peak at 306 nm was used for quantification, using experimentally determined extinction coefficients. Gravimetry was performed by drying the saturated aqueous polyene solutions under vacuum for 24 h on 1 cm^2 pieces of aluminum foil, determining the residual dry weight on a Mettler Toledo MT5 balance with microgram accuracy.

Acknowledgment. We are grateful to Randi Aune for help with shake-flask experiments and fermentations and to Per Bruheim for the TOF-MS data. This work was supported by the Research Council of Norway and Région Rhône-Alpes, France (Thématique Prioritaire de Recherche en Sciences Analytiques Appliquées).

Supporting Information Available: COSY data, ROEs, dihedral angles, and purity data. This material is available free of charge via the Internet at http://pubs.acs.org.

References

(1) Challis, G. L.; Hopwood, D. A. Synergy and contingency as driving forces for the evolution of multiple secondary metabolite production by *Streptomyces* species. *Proc. Natl. Acad. Sci. U.S.A.* **2003**, *100*, Suppl 2, 14555−14561.
(2) Donadio, S.; Staver, M. J.; McAlpine, J. B.; Swanson, S. J.; Katz, L. Modular organization of genes required for complex polyketide biosynthesis. *Science* **1991**, *252*, 675−679.
(3) Brautaset, T.; Sekurova, O. N.; Sletta, H.; Ellingsen, T. E.; Strøm, A. R.; Valla, S.; Zotchev, S. B. Biosynthesis of the polyene antifungal antibiotic nystatin in *Streptomyces noursei* ATCC 11455: Analysis of the gene cluster and deduction of the biosynthetic pathway. *Chem. Biol.* **2000**, *7*, 395−403.
(4) Volchegursky, Y.; Hu, Z.; Katz, L.; McDaniel, R. Biosynthesis of the anti-parasitic agent megalomicin: Transformation of erythromycin to megalomicin in *Saccharopolyspora erythraea*. *Mol. Microbiol.* **2000**. *37*, 752−762.
(5) Molnar, I.; Aparicio, J. F.; Haydock, S. F.; Khaw, L. E.; Schwecke, T.; Konig, A.; Staunton, J.; Leadlay, P. F. Organisation of the biosynthetic gene cluster for rapamycin in *Streptomyces hygroscopicus*: Analysis of genes flanking the polyketide synthase. *Gene* **1996**, *169*, 1−7.
(6) Grimm, A.; Madduri, K.; Ali, A.; Hutchinson, C. R. Characterization of the *Streptomyces peucetius* ATCC 29050 genes encoding doxorubicin polyketide synthase. *Gene* **1994**, *151*, 1−10.
(7) Hopwood, D. A. Genetic contributions to understanding polyketide synthases. *Chem. Rev.* **1997**, *97*, 2465−2498.
(8) Marrakchi, H.; Zhang, Y. M.; Rock, C. O. Mechanistic diversity and regulation of Type II fatty acid synthesis. *Biochem. Soc. Trans.* **2002**. *30*, 1050−1055.
(9) Rock, C. O.; Cronan, J. E. *Escherichia coli* as a model for the regulation of dissociable (type II) fatty acid biosynthesis. *Biochim. Biophys. Acta* **1996**, *1302*, 1−16.
(10) Smith, S.; Witkowski, A.; Joshi, A. K. Structural and functional organization of the animal fatty acid synthase. *Prog. Lipid Res.* **2003**, *42*, 289−317.
(11) Heath, R. J.; Rock, C. O. Roles of the FabA and FabZ beta-hydroxyacyl-acyl carrier protein dehydratases in *Escherichia coli* fatty acid biosynthesis. *J. Biol. Chem.* **1996**, *271*, 27795−27801.
(12) Heath, R. J.; Rock, C. O. Enoyl-acyl carrier protein reductase (fabI) plays a determinant role in completing cycles of fatty acid elongation in *Escherichia coli*. *J. Biol. Chem.* **1995**, *270*, 26538−26542.
(13) Witkowski, A.; Joshi, A. K.; Smith, S. Characterization of the beta-carbon processing reactions of the mammalian cytosolic fatty acid synthase: Role of the central core. *Biochemistry* **2004**, *43*, 10458−10466.
(14) Donadio, S.; Katz, L. Organization of the enzymatic domains in the multifunctional polyketide synthase involved in erythromycin formation in *Saccharopolyspora erythraea*. *Gene* **1992**, *111*, 51−60.
(15) Joshi, A. K.; Smith, S. Construction, expression, and characterization of a mutated animal fatty acid synthase deficient in the dehydrase function. *J. Biol. Chem.* **1993**, *268*, 22508−22513.
(16) Aparicio, J. F.; Caffrey, P.; Gil, J. A.; Zotchev, S. B. Polyene antibiotic biosynthesis gene clusters. *Appl. Microbiol. Biotechnol.* **2003**, *61*, 179−188.
(17) Bolard, J. How do the polyene macrolide antibiotics affect the cellular membrane properties? *Biochim. Biophys. Acta* **1986**, *864*, 257−304.
(18) Volpon, L.; Lancelin, J.-M. Solution NMR structure of five representative glycosylated polyene macrolide antibiotics with a sterol-dependent antifungal activity. *Eur. J. Biochem.* **2002**, *269*, 4533−4541.
(19) Falk, R.; Domb, A. J.; Polacheck, I. A novel injectable water-soluble amphotericin B-arabinogalactan conjugate. *Antimicrob. Agents Chemother.* **1999**, *43*, 1975−1981.
(20) Grzybowska, J.; Sowinski, P.; Gumieniak, J.; Zieniawa, T.; Borowski, E. N-methyl-N-D-fructopyranosylamphotericin B methyl ester, new amphotericin B derivative of low toxicity. *J. Antibiot.* **1997**, *50*, 709−711.
(21) Sambrook, J.; Fritsch, E. F.; Maniatis, T. *Molecular Cloning: A Laboratory Manual*, 2nd ed.; Cold Spring Harbor Laboratory Press: Cold Spring Harbor, NY, 1989.
(22) Flett, F.; Mersinias, V.; Smith, C. P. High efficiency intergeneric conjugal transfer of plasmid DNA from *Escherichia coli* to methyl

DNA-restricting streptomycetes. *FEMS Microbiol. Lett.* **1997**, *155*, 223−229.
(23) Sekurova, O.; Sletta, H.; Ellingsen, T. E.; Valla, S.; Zotchev, S. Molecular cloning and analysis of a pleiotropic regulatory gene locus from the nystatin producer *Streptomyces noursei* ATCC11455. *FEMS Microbiol. Lett*. **1999**, *177*, 297−304.
(24) Rance, M.; Sorensen, O. W.; Bodenhausen, G.; Wagner, G.; Ernst, R. R.; Wuthrich, K. Improved spectral resolution in cosy ^{1}H NMR spectra of proteins via double quantum filtering. *Biochem. Biophys. Res. Commun.* **1983**, *117*, 479−485.
(25) Braunschweiler, L.; Ernst, R. R. Coherence transfer by isotropic mixing: Application to proton correlation spectroscopy. *J. Magn. Reson*. **1983**, *53*, 521.
(26) Davis, D. G.; Bax, A. Assignment of complex ^{1}H NMR spectra via two-dimensional homonuclear Hartmann−Hahn spectroscopy. *J. Am. Chem. Soc*. **1985**, *107*, 2820−2821.
(27) Bax, A.; Davis, D. G. Practical aspects of two-dimensional transverse NOE spectroscopy. *J. Magn. Reson*. **1985**, *63*, 207.
(28) Bothner-By, A.; Stephens, R. L.; Lee, J. M.; Warren, C. D.; Jeanloz, R. W. Structure determination of a tetrasaccharide: Transient nuclear Overhauser effects in the rotating frame. *J. Am. Chem. Soc*. **1984**, *106*, 811−813.
(29) Bax, A. Rapid recordering of 2D NMR spectra without phase cycling. Application to the study of hydrogen exchange in proteins. *J. Magn. Reson*. **1989**, *85*, 393−399.
(30) Pons, J. L.; Malliavin, T. E.; Delsuc, M. A. GIFA V.4: A complete package for NMR data set processing. *J. Biomol. NMR* **1996**, *8*, 445−452.
(31) Bodenhausen, G.; Ruben, D. J. Natural abundance N-15 NMR by enhanced heteronuclear spectroscopy. *Chem. Phys. Lett.* **1980**, *69*, 185−189.
(32) Bachmann, P.; Aue, W. P.; Muller, L.; Ernst, R. R. Phase separation in 2-dimensional spectroscopy. *J. Magn. Reson.* **1977**, *28*, 29−39.
(33) Bax, A.; Summers, M. F. ^{1}H and ^{13}C assignments from sensitivity-enhanced detection of heteronuclear multi-bound connectivity by 2D multiple quantum NMR. *J. Am. Chem. Soc.* **1986**, *108*, 2093−2094.
(34) Cavanagh, J.; Rance, M. Sensitivity enhancement in isotropic mixing (TOCSY) experiments. *J. Magn. Reson.* **1990**, *88*, 72−85.
(35) Palmer, A. G. I.; Cavanagh, J.; Wright, P. E.; Rance, M. Sensivity improvement in proton-detected two-dimensional correlation NMR spectroscopy. *J. Magn. Reson.* **1991**, *93*, 151−170.
(36) Garrett, D. S.; Powers, R.; Gronenborn, A. M.; Clore, G. M. A common-sense approach to peak picking in 2-dimensional, 3-dimensional, and 4-dimensional spectra using automatic computer analysis of contour diagrams. *J. Magn. Reson.* **1991**, *95*, 214−220.
(37) Wüthrich, K. *NMR of Proteins and Nucleic Acids;* Wiley-Interscience, New York, 1986.
(38) Brünger, A. T. *X-PLOR*, version 3.851; Yale University Press: New Haven, CT, 1996.
(39) Koradi, R.; Billeter, M.; Wüthrich, K. MOLMOL: A program for display and analysis of macromolecular structures. *J. Mol. Graph*. **1996**, *14*, 29−32.
(40) Brautaset, T.; Borgos, S. E. F.; Sletta, H.; Ellingsen, T. E.; Zotchev, S. B. Site-specific mutagenesis and domain substitutions in the loading module of the nystatin polyketide synthase, and their effects on nystatin biosynthesis in *Streptomyces noursei*. *J. Biol. Chem*. **2003**, *278*, 14913−14919.
(41) Omura, S.; Tanaka, H. Production, structure, and antifungal activity of polyene macrolides. In *Macrolide Antibiotics: Chemistry, Biology, and Practice;* Omura, S., Ed.; Academic Press: New York, 1984; pp 351−405.
(42) Bruheim, P.; Borgos, S. E. F.; Tsan, P.; Sletta, H.; Ellingsen, T. E.; Lancelin, J.-M.; Zotchev, S. B. Chemical diversity of polyene macrolides produced by *Streptomyces noursei* ATCC 11455 and recombinant strain ERD44 with genetically altered polyketide synthase NysC. *Antimicrob. Agents Chemother*. **2004**, *48*, 4120−4129.
(43) Mazerski, J.; Borowski, E. Molecular dynamics of amphotericin B. II. Dimer in water. *Biophys. Chem.* **1996**, *57*, 205−217.
(44) Milhaud, J.; Michels, B. Binding of nystatin and amphotericin B with sterol-free L-dilauroylphosphatidylcholine bilayers resulting in the formation of dichroic lipid superstructures. *Chem. Phys. Lipids* **1999**, *101*, 223−235.
(45) Coutinho, A.; Silva, L.; Fedorov, A.; Prieto, M. Cholesterol and ergosterol influence nystatin surface aggregation: Relation to pore formation. *Biophys. J.* **2004**, *87*, 3264−3276.
(46) Zotchev, S.; Haugan, K.; Sekurova, O.; Sletta, H.; Ellingsen, T. E.; Valla, S. Identification of a gene cluster for antibacterial polyketide-derived antibiotic biosynthesis in the nystatin producer *Streptomyces noursei* ATCC 11455. *Microbiology* **2000**, *146*, 611−619.

JM050895W